JACS
JOURNAL OF THE AMERICAN CHEMICAL SOCIETY
Article
pubs.acs.org/JACS

Circular Birefringence of Banded Spherulites

Xiaoyan Cui,[†] Alexander G. Shtukenberg,*[,†] John Freudenthal,[†,‡] Shane Nichols,[†] and Bart Kahr*[,†]

[†]Department of Chemistry, New York University, 100 Washington Square East, New York, New York 10003
[‡]Hinds Instruments, 7245 NW Evergreen Parkway, Hillsboro, Oregon 97124

Supporting Information

ABSTRACT: Crystal optical properties of banded spherulites of 21 different compounds—molecular crystals, polymers, and minerals—with helically twisted fibers were analyzed with Mueller matrix polarimetry. The well-established radial oscillations in linear birefringence of many polycrystalline ensembles is accompanied by oscillations in circular birefringence that cannot be explained by the natural optical activity of corresponding compounds, some of which are centrosymmetric in the crystalline state. The circular birefringence is shown to be a consequence of misoriented, overlapping anisotropic lamellae, a kind of optical activity associated with the mesoscale stereochemistry of the refracting components. Lamellae splay as a consequence of space constraints related to simultaneous twisting of anisometric lamellae. This mechanism is supported by quantitative simulations of circular birefringence arising from crystallite twisting and splaying under confinement.

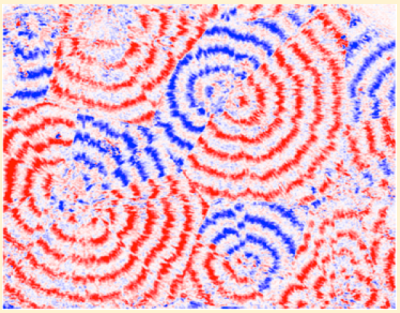

INTRODUCTION

Pattern formation is one of the great organizing principles among all of the sciences.[1−3] For crystallographers, the study of polycrystalline patterns can be a window on the natural world at large. However, chemists have traditionally eschewed polycrystalline patterns because they are not amenable to single-crystal structure analysis by X-ray diffraction, arguably the dominant theme in chemical crystallography in the last century. Nevertheless, ensembles of innumerable tiny crystals may be rich in structure of a different kind, evidenced in the arrangements of crystallites with respect to one another. The study of this kind of structure can and should be a scientific emphasis in and of itself.

The most common polycrystalline pattern is the arrangement of high aspect ratio crystallites in spherulites.[4] Banded spherulites constitute an important subset, in addition to the radial organization of fibrous or plank-like crystals, show concentric rings of varying linear birefringence (LB) in the petrographic microscope.[5] Such structures were first seen in chalcedony, a fibrous form of quartz.[6] This polycrystalline pattern has subsequently been observed in elements,[7] simple salts,[8] organic molecular crystals,[9] and high polymers.[10−13] This oscillating variation in optical properties is now generally recognized as a consequence of helical twisting of fibers or thin lamellae.

While banded spherulites of high-molecular weight polymers (high polymers) have been studied intensively since the 1950s—almost to the exclusion of all other materials—we have recently been emphasizing the study of banded spherulites of simple molecular crystals because such substances can be obtained in high purity, are monodisperse, and are thus well suited to experiments crafted to test mechanisms of crystal twisting. Twisting itself is no longer in dispute, but how it happens is vigorously debated.[5,10]

Optical crystallography is well adapted to the analysis of polycrystalline pattern formation, and we have brought Mueller matrix microscopy to the study of banded spherulites including hippuric acid,[14] mannitol,[15] and aspirin.[16] Mueller matrix microscopy is valuable in this regard because it can simultaneously measure LB, linear dichroism (LD), circular birefringence (CB), and circular dichroism (CD).

Previously, we attributed the large CB in *nonbanded* polymer spherulites[17] to the overlap of misoriented, linearly anisotropic, planklike crystals. Here, we analyze the CB of 25 banded spherulites helically twisted lamellae and conclude that concentric bands of CB of alternating sign (three examples shown in Figure 1) is a near universal optical signature of helical twisting in banded spherulites, whether of small molecules, minerals, or high polymers. CB has long been used to assay molecular structure—enantiomorphism. We emphasize here that optical activity can also be used to assay the mesoscale organization of complex, anisotropic materials.

In the paper to follow, we first describe and tabulate the polarimetric properties of a great variety of banded spherulites and correlate these features with microstructural analysis by electron microscopy. The optical properties are then predicted with the Stokes−Mueller calculus, presuming a mesoscale organization of linearly birefringent lamellae with just one fitted parameter, the lamellae misalignment angle. Finally, a geometrical model is proposed that gives the microstructure so established on the basis of multiple planks twisting in phase under the spatial constraints of a thin film.

Received: February 7, 2014
Published: March 13, 2014

   dx.doi.org/10.1021/ja5013382 | J. Am. Chem. Soc. 2014, 136, 5481−5490

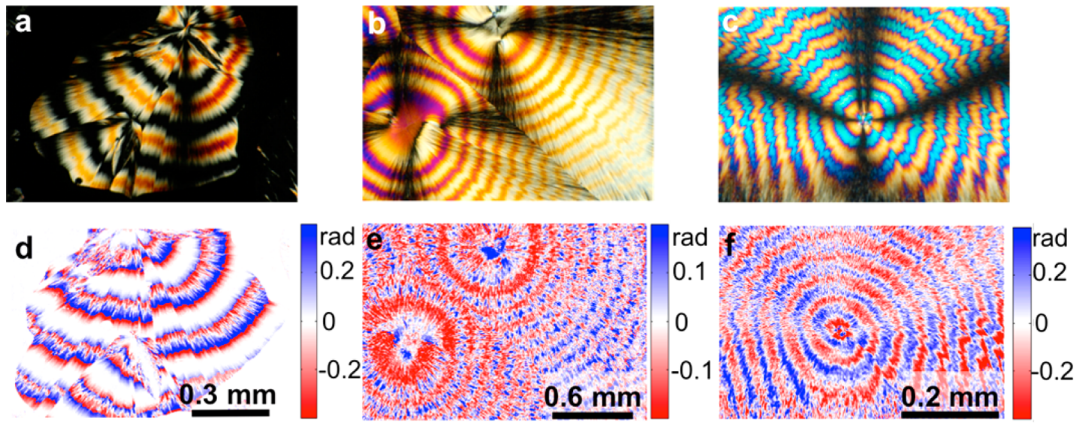

Figure 1. Banded spherulites of urea (a, d), (+)-3-bromocamphor (b, e), and hydroquinone polymorph II (c, f) viewed between crossed polarizers (a, b, c) and their corresponding CB images (d, e, f). As the images in the top and bottom rows were made with different microscopes, the corresponding areas captured are not perfectly coincident.

EXPERIMENTAL SECTION

Crystal Growth. Several milligrams of materials in Table 1 were melted on a Kofler bench between a glass microscope slide and coverslip to form thin films. Supercooled melts were subsequently allowed to crystallize at pre-established temperatures known to given banded spherulitic growth. In order to form spherulites with fine fibers, crystallization typically was performed at high supercooling, sometimes in the presence of resins, polymers, or small-molecule additives.[5] Crystallization is given in Table 1.

Mueller Matrix Microscopy. Optical properties were established with a Mueller matrix microscope, described previously, using a xenon arc lamp and monochromator (micrographs were recorded at $\lambda = 532$ nm but we did not use a laser source).[18] For consistency with the literature, we will use the designations |LB| and CB even when referring to linear and circular *retardance*, respectively, quantities that depend linearly on path length, L, as opposed to thickness invariant refractive index differences. These are given as the following:

$$\mathrm{LB} = 2\pi(n_{0^\circ} - n_{90^\circ})L/\lambda \quad (1)$$

and

$$\mathrm{CB} = 2\pi(n_{\mathrm{L}} - n_{\mathrm{R}})L/\lambda \quad (2)$$

where n_{0° and n_{90° are the refractive indices for orthogonal polarizations, and n_{L} and n_{R} are refractive indices for left and right circularly polarized light.

Atomic Force Microscopy (AFM). Film thicknesses and lamellae cross-sectional sizes were recorded with an Asylum MFP-3D-SA AFM. Measurements were performed in contact mode at deflection −2.0 V on samples with coverslips removed.

Scanning Electron Microscopy (SEM). Samples were mounted on conductive carbon tape, fastened to aluminum holders, and then coated with 5 nm of gold or 4 nm of iridium. The images were recorded with a Carl Zeiss MERLIN field emission scanning electron microscope using a standard Everhart-Thornley type detector with an acceleration voltage of 2−3 kV.

X-ray Diffraction (XRD). Phase identification and crystallite indexing were achieved with a Bruker AXS D8 DISCOVER GADDS X-ray microdiffractometer equipped with a 0.5 mm MONOCAP collimator (Cu Kα radiation) and a VÅNTEC-2000 two-dimensional detector.

RESULTS

Banded spherulites of 21 different substances (25 distinct spherulites if distinguishing polymorphs and radial growth directions) were characterized using Mueller matrix microscopy (Table 1; Figures 1, 2, 4, 5, S2−S17). In all the cases, |LB| oscillates along the growth direction. A direct relationship between optical banding observed in an ordinary petrographic microscope and helicoidal twisting of spherulite fibers was previously observed by the method of "sensing-the-screw,"[9,19−25] whereby the extinction bands move up or down depending on helical sense for a sample rotated around a radius. In the samples studied here, the method of sensing-the-screw was used to establish helicoidal twisting for hippuric acid,[14] tetraphenyl lead,[26] poly(3-hydroxybutyrate) (PHB),[12,27,28] poly(3-hydroxybutyrate-*co*-8 mol %-3-hydroxyhexanoate) (PHBHHx-8)[29] and poly(L-lactic acid) (PLLA).[30] Previously, we have shown that |LB| of aspirin spherulites oscillates with rotation of the optical indicatrix along the growth direction with a constant rate.[15,16] Fiber twisting as the etiology of spherulite banding was established with AFM, SEM, and XRD for α- and δ-mannitol,[15] aspirin,[16] tetraphenyl lead,[26] durene, and chalcedony.[31,32] For other compounds, the presence of twisting was confirmed indirectly by the smooth, sine-like |LB| variations along the spherulite radii.

Compared to LB, extraction and analysis of CB data is more complicated and was achieved for 22 of the 25 types of spherulites. The CB images of chalcedony, itaconic acid, and saccharin show oscillations, but their ragged banding was difficult to interpret. We only list |LB| for these materials in Table 1. Metastable testosterone propionate (TP) shows a smooth |LB| oscillation but no CB oscillation and will be discussed separately. Also, urea, (+)-3-bromocamphor, polymorph II of hydroquinone, saccharin, itaconic acid, chalcedony, *N*-(2-thienylcarbonyl)glycine, and both types of hippuric acid spherulites usually have |LB| higher than the first order. Retardance of multiple orders is not unambiguously defined in the Stokes−Mueller calculus; therefore, the reduced |LB| between 0 and π is reported. For such samples, the absolute value of |LB| can be found by unfolding the measured |LB| when it reaches $n\pi$ (n = 1, 2, 3...). If |LB| exceeds π, the absolute value of CB also requires unwrapping. In a single crystal, it is possible to unfold CB associated with high-order LB,[33] but such algorithms are less hardy for materials that are heterogeneous along the light path and evolving in sample plane.

CB measured for different samples and even for different parts of the same sample can vary significantly. These variations can be related to local microstructural differences or errors in sample alignment. To avoid the latter possibility the reproducibility of the Mueller matrix measurements have been analyzed. The same aspirin sample was mounted, aligned,

dx.doi.org/10.1021/ja5013382 | J. Am. Chem. Soc. 2014, 136, 5481−5490

Table 1. Optical and Crystallographic Properties of the Banded Spherulites

cmpd	figure [ref]	additive/impurity	T_c/T_m,[a] °C	space group	growth direction [*hkl*]	radial LB sign[b]	max/min |LB|	max CB
aspirin	ref 16	salicylic acid, 15 wt %[16]	20/133	$P2_1/C$	[010]	P	2.3/0.6	0.1
(+)-3-bromocamphor	Figure 1b, e	Canada balsam, 10 wt %	20/78	N.D.	N.D.	P	3.6/2.3	0.1[c]
chalcedony	Figure S2	none/unknown	N.D.[D]	$P3_12$	[110][38]	A	4.2/0.5	N.D.
coumarin	Figure S3	Canada balsam, 10 wt %	20/71	N.D.	N.D.	A	1.9/1.1	0.05
1,5-dichloro-2,3-dinitrobenzene, DCDNB	Figure S4	durene, 10 wt %	20/97	$P4_12_12_1$	[*hk*0]	P	1.9/0.2	0.013
durene	Figure 2	gum mastic, 20 wt %	20/79	$P2_1/a$	[100]	N	2.8/1.3	0.12
hippuric acid	Figure S5	none/unknown[14]	70/188	$P2_12_12_1$	[001]	N	4.2/1	0.2[c]
hippuric acid	Figure S6	none/unknown[14]	120/188	$P2_12_12_1$	[100]	A	11/0.2	0.3[c]
hydroquinone (polymorph I)	Figure S7	L-tartaric acid, 20 wt % or Canada balsam, 10 wt %	20/172	N.D.	N.D.	A	2.0/1.5	0.09
hydroquinone (polymorph II)	Figure 1c, f	L-tartaric acid, 20 wt % or Canada balsam, 10 wt %	20/172	N.D.	N.D.	A	8.9/4.6	0.58[c]
iodoform	Figure S8	tribromobenzene, 30 wt %	20/121	$P6_3$	N.D.	A	1.7/1.2	0.04[c]
itaconic acid	Figure S9	Canada balsam, 10 wt %	20/163	N.D.	N.D.	P	5.1/1.8	N.D.
α-mannitol	refs 15,39	polyvinylpyrrolidone, PVP, 15 wt %[15]	95/166	$P2_12_12_1$	[100]	A	0.75/0.35	0.03
δ-mannitol	refs 15,39	Polyvinylpyrrolidone, PVP, 15 wt %[15]	110/155	$P2_1$	[001]	P	1.45/1.15	0.03
N-(2-thienylcarbonyl) glycine	Figure S10	none/unknown	120/167	$P2_12_12_1$	[100]	A	12/0.3	0.08[c]
polycaprolactone, PCL	Figure S11	none/unknown	40/60	$P2_12_12_1$	[010][40,41]	A	1.5/0.2	0.05
poly(3-hydroxy-butyrate), PHB	Figure 4	none/unknown	70/175	$P2_12_12_1$	[010][27]	A	1.0/0.2	0.02
poly(3-hydroxybutyrate-Co-8 mol %-3-hydroxyhexanoate), PHBHHX-8	Figure S12	none/unknown	70/200	$P2_12_12_1$	[010][29]	A	1.8/0.8	0.04
poly(L-lactic acid), PLLA	Figure S13	poly(ethylene oxide), PEO, 20 wt %	90/150	$P2_12_12_1$	[010]	N	1.2/0.05	0.015
resorcinol	Figure S14	L-tartaric acid, 5 wt %[42]	20/110	N.D.	N.D.	A	0.7/0.15	0.01
saccharin	Figure S15	Canada balsam, 20 wt %	80/229	N.D.	N.D.	A	7.2/0.9	N.D.
testosterone propionate, TP (stable form)	Figure S16	none/unknown[43]	60/120	$P2_12_12_1$	[100]	A	2.7/0.6	0.11
testosterone propionate, TP (metastable form)	Figure 5	none/unknown[43]	4/120	N.D.	N.D.	A	1.0/0.05	0.08
tetraphenyl lead	Figure S17	polyvinylpyrrolidone, PVP, 39 wt %[26]	150−170/225	$P\bar{4}2_1c$	[100]	P	1.8/0.5	0.08
urea	Figure 1A, D	Canada balsam, 20 wt %	20/133	$P\bar{4}2_1m$	N.D.	N	6.0/0.04	0.4[c]

[a] T_c - crystallization temperature, T_m - melting point, N.D. - not determined. [b] P - positive spherulites, N - negative spherulites, A - spherulites with alternating sign of LB along the radius. [c] Absolute CB values were not determined due to high |LB|.

and measured five times. For the same 255-point profile extracted from the data, the averaged standard deviations per point was 0.018 rad for |LB| and 0.003 rad for CB with oscillations between 0.3 and 2.7 rad and 0.02 and 0.17 rad, respectively (Figure S18 in SI). This confirms that measured differences arise in local microstructure. For example Figure S19 in SI shows |LB| and CB profiles measured along seven radial directions for one aspirin spherulite. The profiles of |LB| and CB look similar but not exactly the same. In particular, maximum values of |LB| and CB vary in the range 2.70(9) rad and 0.13(3) rad, respectively.

In the banded spherulites investigated, CB oscillates with a period equal to that of |LB| (π rotation of crystallites or pitch, *P*). The CB distribution within a period varies, however. As was found earlier for α- and δ-mannitol,[15] CB shows almost sine-like oscillations with positive and negative extremes of almost equal magnitude. Zero CB corresponds to |LB| maxima and minima and coincides with edge-on and flat-on orientations of the lamellae.

In contrast, aspirin spherulites are roughly divided into heterochiral halves where CB in each hemicircle oscillates between ∼zero and either a positive or negative value, respectively.[16] The aspirin domains correspond to a left (negative CB)- and right (positive CB)-handed sense of twisting for the opposite enantiopolar[34] ⟨010⟩ growth directions of aspirin crystallites with monoclinic 2/*m* symmetry.[16] As for mannitol, zero CB corresponds to edge-on and flat-on orientations of the lamellae. The differential effect of circularly polarized light in the presence of heterochiral

dx.doi.org/10.1021/ja5013382 | J. Am. Chem. Soc. 2014, 136, 5481−5490

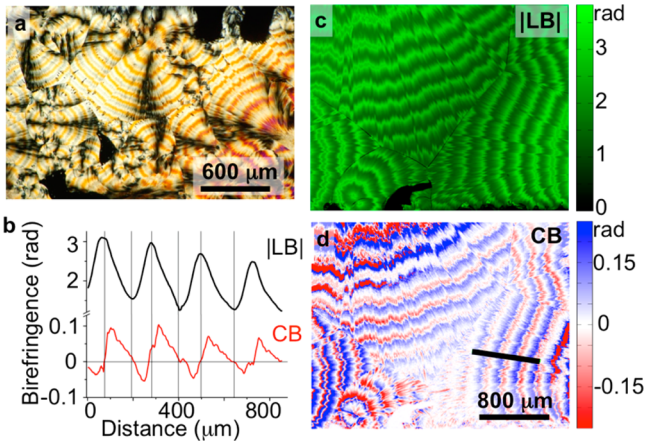

Figure 2. (a) Durene spherulites viewed between crossed polarizers. (c, d) |LB| and CB false color micrographs and (b) extracted optical properties along the fiber growth direction (black line in (d)). λ = 532 nm.

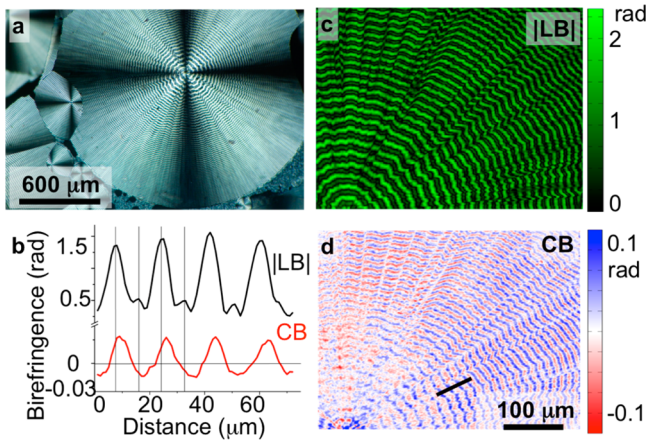

Figure 4. (a) PHB spherulites between crossed polarizers. (c,d) |LB| and CB false color micrographs. (b) Optical data extracted along growth direction (black line in (d)).

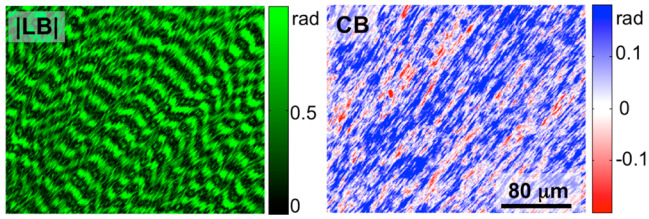

Figure 5. |LB| and CB false color micrographs of metastable form of TP spherulites.

mesotextural domains was seen previously in films of phthalic acid spherulites.[35]

Here, we have carried out detailed analysis of durene, which also crystallizes with 2/*m* symmetry.[36] In the presence of gum mastic, durene forms banded spherulites where the smallest refractive index is radial (Figure 2a). XRD analysis showed that durene crystallites grow along ⟨100⟩. CB oscillations are asymmetric along the growth direction. SEM shows that durene lamellae are ∼300 nm thick but 10 times wider (Figure 3). As lamellae twist, their orientations gradually alternate between edge-on and flat-on. Comparison of SEM and optical data shows that edge-on regions are characterized by the highest

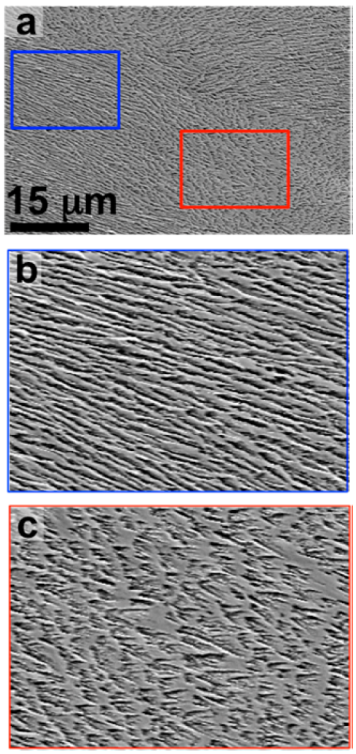

Figure 3. (a) SEM image of a durene spherulite and enlarged areas of edge-on (b, blue box in (a)) and flat-on (c, red box in (a)) lamellae.

|LB| and zero CB (Figure 2b), whereas flat-on regions have the smallest |LB| and zero CB. Durene CB has sawtooth modulation, as opposed to sinusoidal.

We did not study microstructures of polymer spherulites by AFM or SEM but it is well-known that PHB, PHBHHx-8, PLLA, and polycaprolactone (PCL) crystallize in the orthorhombic space group $P2_12_12_1$ and form ⟨010⟩ elongated lamellae with very anisotropic cross sections (width to thickness aspect ratio is up to 100:1).[13,27,37] The larger dimension corresponds to {100} folding surfaces, whereas the smaller dimension is bounded by {001}. Thus, in accordance with symmetry 222, edge-on and flat-on orientations should correspond to |LB| extrema. Comparisons of |LB| and CB profiles for PHB (Figure 3b), PHBHHx-8 (Figure S12 in SI), and PLLA (Figure S13 in SI) show that edge-on and flat-on orientations are absent CB, in agreement with all previous samples.

|LB| and CB are trivially correlated since they both depend linearly on thickness (eqs 1 and 2). We further analyzed whether CB also depends on pitch, *P*. In banded spherulites, *P* usually decreases with growth temperature.[9,26] For tetraphenyl lead, such variations can be significant (P = 17, 30, and 50 μm), yet |LB| was 1.7−1.8 rad and CB was constant as well (0.04−0.05 rad).

Of the materials in Table 1, only two did not show |LB| and CB oscillations. In phthalic acid, |LB| oscillations are principally the result of rhythmic precipitation but not fiber twisting.[35] Hemicircles show oppositely signed CB (Figure S1 in SI) and in this regard resemble aspirin.[16] Overlapped crystallites with a stereospecific sense likely account for this optical enantiomorphism, even in the absence of continuous twisting.

dx.doi.org/10.1021/ja5013382 | J. Am. Chem. Soc. 2014, 136, 5481−5490

The second exclusion is the metastable polymorph of TP.[43] The |LB| gives a typical banded structure, while CB does not oscillate. Polarized light microscopy[43] shows that the fiber cross sections of TP are cylindrical rather than lamellar as is common for other substances. (SEM and AFM analyses could not be made due to the instability of the polymorph at room temperature). As discussed below, the shape of the fibers is crucial in establishing the alternating CB. The CB signal is nevertheless large and predominantly monosignate (see Discussion).

DISCUSSION

Key Observations. All banded spherulites examined here are characterized by the following optical and structural features that should be reproduced by any model of the data: (1) Continuous helicoidal twisting of spherulite fibers provides |LB| and CB oscillations; (2) |LB| and CB oscillation periods are the same; (3) |LB| and CB oscillations can be in phase or out of phase by a fixed offset; (4) |LB| almost always shows sine-like oscillations, whereas CB profiles vary; (5) samples with high |LB| usually have high CB; (6) edge-on and flat-on orientations of lamellae have zero CB; (7) for the same material, opposite twist sense accompanies opposite signs of CB.

Sources of CB. CB is most familiar as a manifestation of the natural optical activity of dissymmetric molecules in solution. Natural optical activity is not the principal source of CB in banded spherulites here. Some of our crystalline materials are centrosymmetric and cannot have natural optical activity (Table 1). For others, CB is much larger than what is anticipated from natural optical activity. Typical values of nonresonant optical rotation ρ of molecular crystals are less than $\pm 100°$/mm ($\rho = -56°$/mm for β-mannitol;[44] $\rho \approx -40°$/mm for tetraphenyl lead;[45] $\rho = 11°$/mm for PHB[46]). The upper limit of $\rho = 100°$/mm for a typical sample thickness of $L = 2$ μm gives CB = 0.004 rad (CB = 2ρ), much smaller than the observed values (0.01−0.2 rad) in banded spherulites in Table 1.

More likely, the origin of CB can be explained via superimposition of misoriented crystallites. This mechanism is consistent with the very first model of optical rotation, Reusch's pile of misoriented mica plates.[47,48] Reusch was able to mimic optical rotation in crystals by stacking flakes of mica, each rotated in the same sense by a small angle from layer to layer. CB as a consequence of misoriented anisotropic lamellae has been observed in other systems.[17,18,35] In spherulites, individual fibers are often plank-like with large width-to-thickness aspect ratios. Lamellae thicknesses typically range from 50 to 500 nm for molecular crystals and from 5 to 20 nm for high polymers. The width of lamellae is 0.3−2 μm. Light traversing a typical 1.5−7-μm thick sample will interact with at least several overlapping lamellae for all orientations, except those close to edge-on. If lamellae are exactly parallel, CB will be zero, but a slight misorientation can give a strong optical response, especially if the layers are highly anisotropic.

Model. To verify if the CB patterns observed originate from the superimposition of overlapped lamellae, we simulated the optical response. We built Mueller matrices (M_k, $k = 1,2...N$) of identical crystalline plates with the same linear birefringence (LB/N) and progressively rotated them in the same sense by the angle $\varphi/(N-1)$

$$M_k = M_{\mathrm{rot}(k)}^{-1} M_1 M_{\mathrm{rot}(k)},\ k = 2,\ 3...N \tag{3}$$

where

$$M_1 = \begin{bmatrix} 1 & 0 & 0 & 0 \\ 0 & 1 & 0 & 0 \\ 0 & 0 & \cos(\mathrm{LB}/N) & \sin(\mathrm{LB}/N) \\ 0 & 0 & -\sin(\mathrm{LB}/N) & \cos(\mathrm{LB}/N) \end{bmatrix}$$

and

$$M_{\mathrm{rot}(k)} = \begin{bmatrix} 1 & 0 & 0 & 0 \\ 0 & \cos(k\varphi/(N-1)) & -\sin(k\varphi/(N-1)) & 0 \\ 0 & \sin(k\varphi/(N-1)) & \cos(k\varphi/(N-1)) & 0 \\ 0 & 0 & 0 & 1 \end{bmatrix}$$

A product of N Mueller matrices describes the optical response of an ensemble of progressively misoriented lamellae:

$$M_{\mathrm{total}} = \prod_{k=1}^{N} M_k = \begin{bmatrix} m_{00} & m_{01} & m_{02} & m_{03} \\ m_{10} & m_{11} & m_{12} & m_{13} \\ m_{20} & m_{21} & m_{22} & m_{23} \\ m_{30} & m_{31} & m_{32} & m_{33} \end{bmatrix} \tag{4}$$

Finally, CB can be calculated as:[49,50]

$$\mathrm{CB} = \frac{(m_{12} - m_{21})\ \mathrm{acos}\left(\frac{\mathrm{Tr}(M_{\mathrm{total}})}{2} - 1\right)}{2\sin\left(\mathrm{acos}\left(\frac{\mathrm{Tr}(M_{\mathrm{total}})}{2} - 1\right)\right)} \tag{5}$$

Simulations require three input parameters: the total |LB|, the total misorientation angle φ, and number of lamellae N along the optical path. We make use of the following additional assumptions: (1) Misalignment of overlapping lamellae is the only source of the CB (we presume that additional contributions of natural optical activity in symmetry permitting crystals is a small, secondary effect); (2) At each point, light traverses a stack of misaligned lamellae, yet we ignore multiple scattering from interfaces; (3) Every pair of neighboring lamellae is misoriented by the same angle $\varphi/(N-1)$; (4) Along the fiber elongation direction z the total misalignment angle φ oscillates from zero for the edge-on and flat-on orientations to $\varphi_{\max}$ and $\varphi_{\min} = -\varphi_{\max}$ for two alternating intermediate orientations of lamellae that occur in one-half twisting period, π. The sine function

$$\varphi(z) = \varphi_{\max}\sin(\pi(z - z_0)/P) \tag{6}$$

where z_0 is the position of the edge-on orientation. Equation 6 presumes a smooth sinusoidal oscillation satisfying the aforementioned conditions (Figure 6).

According to this model, CB will increase sharply with φ or |LB| (Figure 7). On the other hand, CB decreases appreciably with the increasing number of layers when $N < 5$ (Figure 7b). For $N > 50$, CB is nearly constant. Since N is known from AFM and SEM, and |LB| is an independently measured experimental quantity, the only fitted parameter in the model is the overall misorientation angle, $\varphi_{\max}$.

Simulations. Simulations have been carried out for δ-mannitol,[15] aspirin,[16] durene (Figures 2, 3), and PHB (Figure 4) with well-resolved CB oscillations and microstructure. With the misorientation angle expressed as eq 6, an excellent fit for all four compounds (Figure 8) was achieved. These one-parameter fits reproduce not only the phase, magnitude, and

dx.doi.org/10.1021/ja5013382 | J. Am. Chem. Soc. 2014, 136, 5481−5490

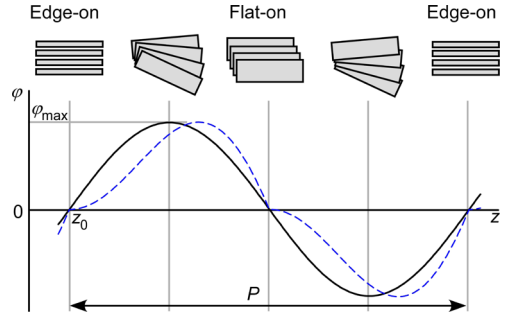

Figure 6. Models of misalignment angle $\varphi(z)$. Simulations in accordance with eq 6 (black solid line) and eq 8 (broken blue line).

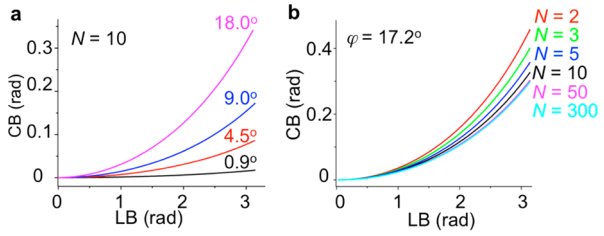

Figure 7. Simulation of CB as a function of |LB|. (a) A series of misorientation angles φ over $N = 10$ layers, and (b) a series of N misoriented lamellae with constant misorientation angle $\varphi = 17.2°$.

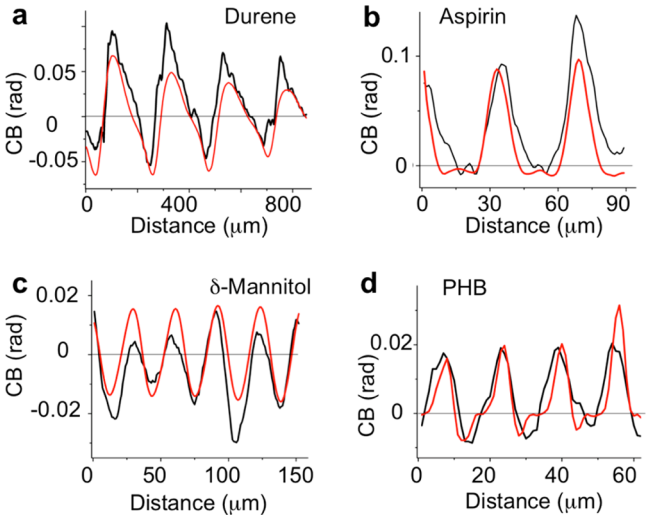

Figure 8. Experimental (black lines) and simulated (red) CB of (a) durene, (b) aspirin, (c) δ-mannitol and (d) PHB as a function of distance along the fiber, z. Misorientation angle was calculated in the form of eq 6. Parameters: (a) $N = 10$; $\varphi_{max} = 16.2°$; (b) $N = 10$; $\varphi_{max} = 10.8°$; (c) $N = 10$; $\varphi_{max} = 5.4°$; (d) $N = 50$; $\varphi_{max} = 17.6°$.

overall shape of oscillations but also small maxima in the regions with CB < 0 for aspirin (Figure 8b) and shoulders for PHB and durene (Figure 8a,d).

Qualitative Analysis of Misalignment. Simulations show that the simple sinusoidal oscillation model of φ reproduces the CB oscillations. Slight disagreements between predicted and simulated CB profiles can be attributed to the approximate character of eq 6, to fluctuations in $\varphi(z)$, and to the fact that not all lamellae twist precisely in phase.

What is the basis for the oscillatory $\varphi(z)$? As outlined previously,[15,16] simultaneous spatial restrictions on in-phase twisting of tightly packed lamellae (Figure 9) alter lamellae

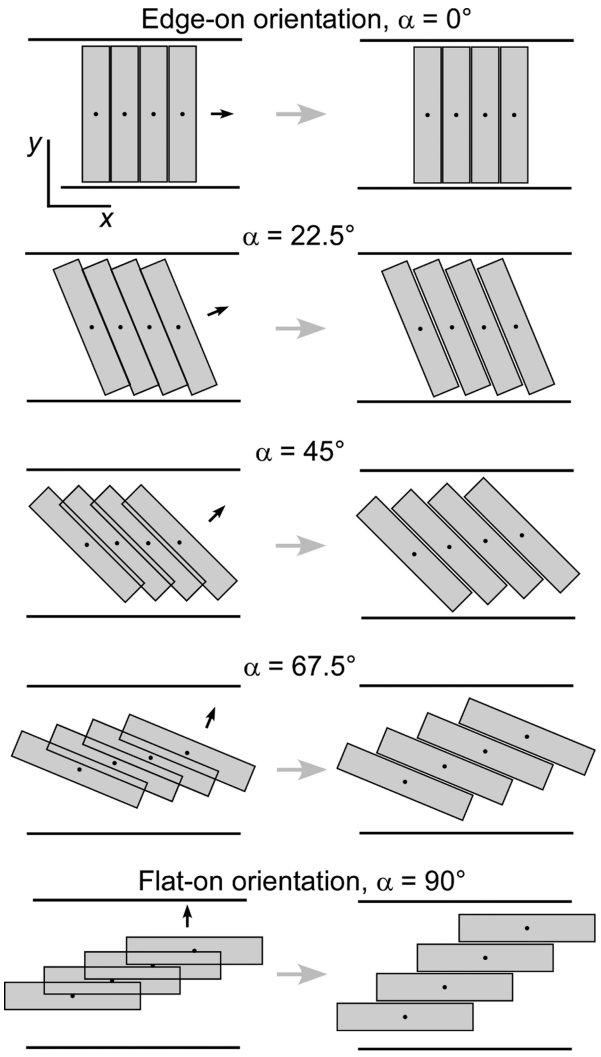

Figure 9. Sketch of a spherulite cross section normal to the growth direction z (rotation angle $\alpha = \pi z/P$). Thick horizontal lines symbolize bottom and upper glass slides between which the spherulite has grown. Left column represents pure rotation of lamellae (gray rectangles) around their centers (black dots), whereas right column shows the end positions that include adjustment of lamellae positions due to splaying. Displacement direction is indicated by black arrows.

trajectories and result in splay. Assume an array of identical lamellae in edge-on orientations ($z = z_0 = 0$; orientation $\alpha = z\pi/P = 0°$ in Figure 9). In the course of twisting, lamellae rotate around their spines (Figure 9). The length of lamellae projected onto the x-axis increases, resulting in lamellae collisions. Flexible lamellae can avoid such collisions by adjusting their positions in space. The shortest path out of harm's way is in the direction normal to the lamella side surface (shown by black arrows in Figure 9). These translations lead to lamellae divergence or splaying. Splaying in the xz plane defines the misorientation angle,

$$\frac{\varphi(z)}{N_I(z)} = \frac{dx}{dz} = \frac{dx}{d\alpha}\frac{\pi}{P} \tag{7}$$

responsible for CB generation. The number of lamellae interfaces within the sample along the optical path, $N_I(z)$, varies from zero for the edge-on orientation to $N - 1$ for the flat-on orientation. The analysis above considers only one pair

dx.doi.org/10.1021/ja5013382 | J. Am. Chem. Soc. 2014, 136, 5481−5490

of lamellae, whereas the value of φ used to fit the data corresponds to the entire path containing N lamellae.

Figure 9 shows CB is minimum for both edge-on and flat-on orientations but for different reasons. In the first instance, the number of interlamellae interfaces traversed by the light path is zero. In the latter case, the displacements occur in parallel to the optical path, y, rather than along x, and thus have no optical consequences. The biggest values of CB should be, and are, observed only for regions *between* edge-on and flat-on orientations.

One must conclude that the sign of φ and the sign of CB have to be opposite for (1) edge-on → flat-on and flat-on → edge-on twisting sequences, and (2) for the opposing senses of twist. The first observation applies to all spherulites (Table 1, Figure 8) except aspirin whose CB oscillates between high positive (negative) and small negative (positive) values. This apparent discrepancy reflects that the flat-on → edge-on regions correspond to a minimum in |LB| (close to zero) and, consequently, CB must also be close to zero since it arises from the misorientations of optical indicatrices (refractive index ellipsoids) in adjacent lamellae. In aspirin,[16] the fiber elongation directions are perpendicular to the crystal mirror plane. Spherulites form from a nucleus that undergoes multiple branching with subsequent geometric selection.[4] Because the nucleus grows in opposite directions, spherulites eventually consist of two parts evolved from opposite ends of the original crystal nucleus that twist in opposite directions.[5] The observed sign of CB correlates with the sense of twisting observed by SEM (Figure 10).[16]

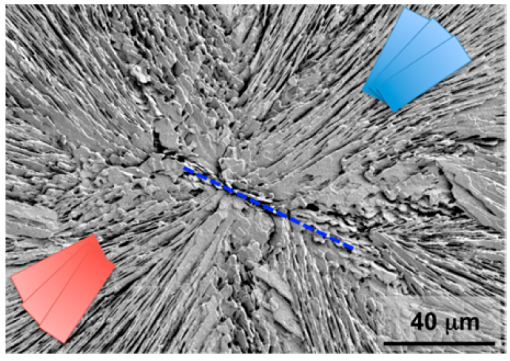

Figure 10. SEM image of aspirin spherulites. Blue dashed line indicates the interface separating opposing growth directions in opposite hemispheres; the rectangles highlight the opposite senses of twist; red and blue colors correlate with CB signs elsewhere.

Near flat-on orientations, the arrangement of twisted lamellae is complex, and the simple splaying mechanism illustrated in Figure 9 must be refined. Foremost, not all lamellae twist in phase. Those leading in the transition from edge-on to flat-on are less encumbered and have the capacity to widen (sometimes up to 5−10 times[15]). Widening, leading lamellae collide with the bounding glasses as they twist. The adjacent layers can now assume the leadership positions (Figure 11). They too widen and eventually collide with the glass. Due to this dynamic, lamellae spines or midlines rise and fall out of the xz plane Figure 9. This complicates the microstructure of aspirin spherulites (Figure 11) described below and seen in mannitol (Figure 9a in ref 15 and Figure S20 in SI). Moreover, the xy displacements lead to lamellae bunching (Figure 11) accompanied by strong branching, for example at points

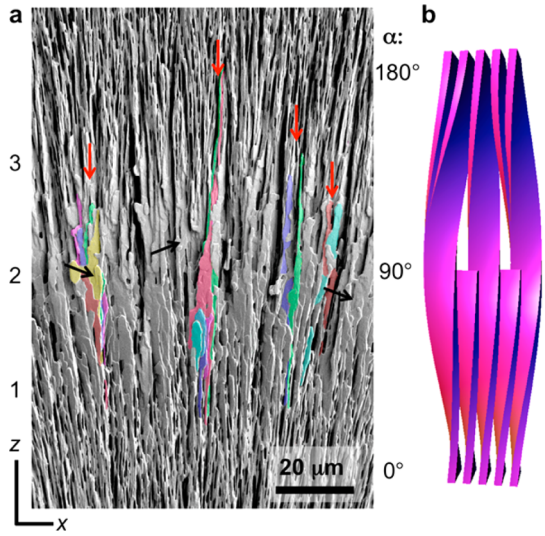

Figure 11. (a) SEM of twisted aspirin lamellae with false color highlighting individual fibers. The growth direction corresponds to $+z$. The numbers to the left of the image highlight the regions of different lamella orientation. (1) Lamellae have intermediate positions between edge-on and flat-on orientations. (2) Close to flat-on lamellae widen. The top- and bottom-most lamella must stop growing when they collide with the glasses (top coverslip obviously removed for SEM). Just after the flat-on orientation only some lamellae can continue growth, forming bundles. Lamellae then branch. One branch can continue twisting having jettisoned some of its width (several branching points are designated by black arrows). (3) Lamellae have intermediate positions between flat-on and edge-on orientations. Different groups of colored lamellae are labeled by red arrows. (b) Scheme of one bundle of twisted lamellae that highlights cessation of growth follow by branching to give new lamellae.

indicated in Figure 11 by black arrows. New branches may collide with glass surfaces and stop growing (second red arrow in Figure 11); others continue but in slightly different directions and ultimately become associated with the same bundle or another. The trajectories of lamellae in a bundle may remain parallel in the case of lateral collisions (Figure 11, colored lamellae below the third red arrow from left) or cross each other (Figure 11 colored lamellae below first, second, and fourth red arrows). In the latter case, the bundle resembles a twisted rope (Figure 11) as has been observed for helical nanofilaments of some liquid crystal phases.[51−53] However, this resemblance is infelicitous. Ropes would give monosignate CB, rather than alternating signs. The cartoon in Figure 11b captures the twisting in a bundle, the demise of a pair of lamellae due to twisting induced constrictions, and ultimately the branching to fill the gaps.

Generally, micrographs tend to accentuate splaying. While crystallographic reorientations by φ are comparatively small, lamellae appear to grossly bend in the xz plane because of asymmetric lamellae widening; one side can grow while the other is obstructed.

Numerical Simulations of Misalignment. The rotation and subsequent displacement of lamellae has been embodied in a numerical algorithm. As applied to a pair of lamellae in Figure 12, the center of the first lamella was fixed at $O(0,0)$ and displacement of the second lamella to points A, B, and C was analyzed. The total turn from edge-on to flat-on orientations ($P/2$ period; Figure 6) was divided into K steps labeled below

dx.doi.org/10.1021/ja5013382 | J. Am. Chem. Soc. 2014, 136, 5481−5490

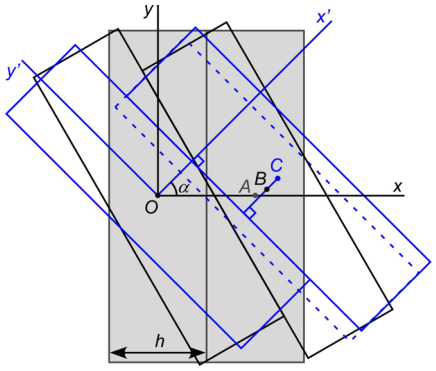

Figure 12. Twisting and splaying geometries used for derivation of eq 8

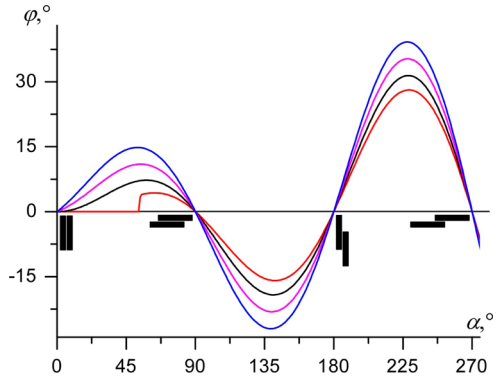

Figure 13. Calculated misorientation angle, φ, as a function of lamellae orientation, α. Number of lamellae $N = 10$; width of lamellae $h = 0.2$ μm; pitch $P = 20$ μm. Simulations start at $\alpha = 0$, where all lamellae have edge-on orientations. Red, black, magenta, and blue lines correspond to initial coordinates of the center of the second lamella $A(h,h/2)$, $A(h,0)$, $A(h,-h/2)$, and $A(h,-h)$, respectively. Abrupt change in red curve reflects that, for this initial configuration, twisting does not initiate collisions for the first 50° of rotation. Pairs of black bars at ~0°, 90°, 135°, and 180° represent increasing displacement of lamellae for each successive exchange of edge-on and flat-on orientations.

by subscript i so the angle of lamellae rotation can be written as $\alpha_i = \pi z_i/P$.

The algorithm expresses the displacement Δx for the arbitrary step i to $i + 1$. Point $B(x_i,y_i)$ marks the central position of the second lamella after rotation α_i (lamellae corresponding to orientation i are black). Similarly, the orientation after rotation by α_{i+1} is shown by the blue lamellae. The dashed line shows the orientation of the second lamella after rotation $\Delta\alpha = \alpha_{i+1} - \alpha_i$ around point $B(x_i,y_i)$ before splaying; the solid line shows the final position with a new center at $C(x_{i+1},y_{i+1})$ (Figure 12). To calculate C, the coordinate system is rotated counterclockwise by α_{i+1}. In the new frame, B has coordinates (x'_i,y'_i). Splaying transforms $B(x'_i,y'_i)$ to $C(x'_{i+1},y'_{i+1})$ with the ordinate $y'_{i+1} = y'_i$ and abscissa $x'_{i+1} = h$ if $x'_i < h$ and $x'_{i+1} = x'_i$ otherwise. The final coordinates $C(x_{i+1},y_{i+1})$ can be obtained by the subsequent clockwise rotation of the coordinate system by α_{i+1}. The misorientation angle can be obtained by substituting $\Delta x_{i+1} = x_{i+1} - x_i$ into eq 7

$$\varphi_{i+1} = (N_l)_{i+1}\frac{\xi|x_{i+1} - x_i|}{z_{i+1} - z_i} = \frac{2\xi K(H - h)|\Delta x_{i+1}\cdot\sin\alpha_{i+1}|}{hP} \quad (8)$$

Here the factor $(N_l)_{i+1} = (N - 1)|\sin\alpha_{i+1}|$ is an approximate correction for the number of lamellae interfaces light traverses for a given position i+1. Misorientation is assumed to be zero for edge-on orientations and $(H - h)/h$ for flat-on orientations, where $H = Nh$ is the sample thickness. Δx_{i+1} in eq 8 is taken as an absolute value because this algorithm does not provide the correct CB sign, and for the same value of Δx_{i+1}, the calculated φ_{i+1} gets the opposite sign, depending on which lamella in the pair moves. The CB sign depends on whether the lamella is above or below the immobile one. To get the correct sequence of signs the factor ξ is introduced: $\xi = 1$ if $(n - 0.5)\pi < \alpha < n\pi$ and $\xi = -1$ if $n\pi < \alpha < (n + 0.5)\pi$; where n is an integer.

Recursive application of this procedure starting from any α_0 and coordinates of the second lamella $A(x_0,y_0)$ gives the whole set of misorientation angles for any given number of steps i (Figure 13). Figure 13 shows the idealized evolution of φ between two twisting lamellae with a sine-like $\varphi(\alpha)$ but with maxima slightly displaced toward larger α. Because φ_{max} is sensitive to the initial coordinates of point A, modeling should be restricted to $0° < \alpha < 90°$. As shown in the previous section, near flat-on orientations, lamellae centers move a lot, and many lamellae undergo renucleation under the constraints of space (Figure 11). Moreover, the distance between centers of lamellae continuously increases as does φ_{max} (Figure 13). For example, at $\alpha = 360°$ it becomes ~$6h$, a distance inconsistent with experiment; y and x are approximately constant for edge-on and flat-on orientations, respectively. For every edge-on and flat-on orientation, all lamellae have their centers aligned parallel and perpendicular to the glass surface, respectively.

In order to cover a half-twist period, we calculated $\varphi_{max}(\alpha)$ for $0° < \alpha < 90°$ with the initial condition $A(h,0)$ at $\alpha = 0°$ and for $90° < \alpha < 180°$ with the initial condition $A(0,h)$ at $\alpha = 90°$. Results of modeling are shown in Figure 6. Within such restrictions and given that φ_{max} depends only on h, N, and P, numerical simulations show that φ_{max} can be approximately expressed (in degrees) as

$$\varphi_{max} = 81(H - h)/P \quad (9)$$

Equation 9 predicts φ_{max} reasonably well for compounds with known lamellae morphologies (Table 2; Figure 8). In accordance with eq 9 compounds with very large pitch (minimal twisting) are optically inactive. δ-Mannitol shows the best correspondence with φ_{max}. Aspirin and PHB are slightly worse. On the other hand, durene, with a comparatively large pitch, deviates considerably. This observation along with pitch-independent CB for tetraphenyl lead ($17 < P < 50$ μm, see above) stable polymorph of TP and DCDNB indicates that the effect of pitch may be more complex than predicted by eq 9.

In general, our model is able to predict the oscillatory misorientation angle and the correct order of φ_{max} magnitude. Given that the model ignores the effects of bounding glass surfaces does not account for the fact that not all lamellae twist in phase[15] (e.g., in Figure 3b not all lamellae are flat-on, some show edge-on orientation) and uses the simplest arrangement of centers of lamellae, agreement with micrographs is favorable.

■ CONCLUSIONS

The arrangement of helicoidally twisted crystalline lamellae in spherulites was established by a combination of optical, electron, and scanning probe microscopies. Mueller matrix imaging performed for 21 materials including molecular crystals, high polymers, and inorganic chalcedony revealed that radial oscillations in |LB|, an obvious consequence of the twisting process that periodically exchanges refractive index

dx.doi.org/10.1021/ja5013382 | J. Am. Chem. Soc. 2014, 136, 5481−5490

Table 2. Comparison of Misorientation Angles φ_{max} Evaluated from Fitting CB and from Eq 9 Using Experimental Sample Thickness, Lamellae Thickness, and Pitch

cmpd	Figure	sample thickness H, μm	lamellae thickness h, μm	pitch P μm	number of lamellae $N = H/h$	φ_{max}° from eq 9	φ_{max}° from fit to data
durene	6a	2.6	0.3	180	9	1.0	16.2
δ-mannitol	6b	2	0.2	30	10	4.9	5.4
aspirin	6c	1.6	0.16	37	10	3.2	10.8
PHB	6d	n.d.	0.007[a]	18	300[b]	9.5	17.6

[a]Experimental data for the sample grown at the same temperature and having similar pitch.[5] [b]This approximate value was obtained by assuming reasonable sample thickness of H = 2.1 μm.

directions, are almost always accompanied by oscillations in CB, a surprising phenomenon having nothing to do with intrinsic optical activity of corresponding compounds. The observed CB was explained on the basis of smoothly oscillating lamellae misorientations. Space constraints among twisting lamellae drive splaying. CB patterns were simulated using a model with one fitting parameter, the maximum misorientation angle, φ_{max}, that can be simply estimated from sample thickness, lamellae thickness, and the twist period. The artificial CB detected in banded spherulites is an optical assay for the determination of twisting and its handedness in banded spherulites.

■ ASSOCIATED CONTENT

Supporting Information

Pages S3–S21: |LB| and CB of 19 banded spherulites; S22: False colored AFM of mannitol banded spherulites. This material is available free of charge via the Internet at http://pubs.acs.org.

■ AUTHOR INFORMATION

Corresponding Authors

shtukenberg@mail.ru
bart.kahr@nyu.edu

Notes

The authors declare no competing financial interest.

■ ACKNOWLEDGMENTS

B.K. thanks the NSF (CHE-0845526, DMR-1105000) for financial support. The authors acknowledge Dr. Chunhua Hu, the NYU Department of Chemistry X-ray Diffraction Facility, and the NSF Chemistry Research Instrumentation and Facilities program (CHE-0840277) for the powder micro-diffractometer. The scanning electron microscope was purchased with financial support from the NSF Major Research Instrumentation program (DMR-0923251). We thank Professor Michael D. Ward for the use of his atomic force microscopes. We thank Drs. Oriol Arteaga and Hai-Mu Ye for very helpful discussion.

■ REFERENCES

(1) Hoyle, R. B. *Pattern Formation*; Cambridge University Press: Cambridge, UK, 2006.
(2) Ball, P. *The Self-Made Tapestry*; Oxford University Press: Oxford, UK, 2001.
(3) Thompson, D. W. *On Growth and Form*; Cambridge University Press, Cambridge, UK, 1942.
(4) Shtukenberg, A. G.; Punin, Yu. O.; Gunn, E.; Kahr, B. *Chem. Rev.* **2012**, *112*, 1805.
(5) Shtukenberg, A. G.; Punin, Y. O.; Gujral, A.; Kahr, B. *Angew. Chem., Int. Ed.* **2014**, *53*, 672.
(6) Michel-Lévy, A.; Munier-Chalmas, C. P. E. *Bull. Soc. Fr. Miner.* **1892**, *15*, 159.
(7) Bolotov, I. E.; Kleptsova, G. N.; Mel'nikov, P. S. *Sov. Phys.: Crystallogr.* **1971**, *16*, 327.
(8) MacMasters, M. M.; Abbott, J. E.; Peters, C. A. *J. Am. Chem. Soc.* **1935**, *57*, 2504.
(9) Bernauer, F. *"Gedrillte" Kristalle*; Bornträger: Berlin, 1929.
(10) Lotz, B.; Cheng, S. Z. D. *Polymer* **2005**, *46*, 577.
(11) Keller, A. *J. Polym. Sci.* **1959**, *39*, 151.
(12) Barham, P. J.; Keller, A.; Otun, E. L.; Holmes, P. A. *J. Mater. Sci.* **1984**, *19*, 2781.
(13) Ye, H.-M.; Wang, J.-S.; Tang, S.; Xu, J.; Feng, X.-Q.; Guo, B.-H.; Xie, X.-M.; Zhou, J.-J.; Li, L.; Wu, Q.; Chen, G.-Q. *Macromolecules* **2010**, *43*, 5762.
(14) Shtukenberg, A. G.; Freudenthal, J.; Kahr, B. *J. Am. Chem. Soc.* **2010**, *132*, 9341.
(15) Shtukenberg, A. G.; Cui, X.; Freudenthal, J.; Gunn, E.; Camp, E.; Kahr, B. *J. Am. Chem. Soc.* **2012**, *134*, 6354.
(16) Cui, X.; Rohl, A. L.; Shtukenberg, A. G.; Kahr, B. *J. Am. Chem. Soc.* **2013**, *135*, 3395.
(17) Ye, H.-M.; Xu, J.; Freudenthal, J.; Kahr, B. *J. Am. Chem. Soc.* **2011**, *133*, 13848.
(18) Freudenthal, J. H.; Hollis, E.; Kahr, B. *Chirality* **2009**, *21*, E20.
(19) Wallerant, F. *C.R. Acad. Sci. (Paris)* **1906**, *143*, 553.
(20) Wallerant, F. *C.R. Acad. Sci. (Paris)* **1906**, *143*, 1169.
(21) Wallerant, F. *Bull. Soc. Fr. Mineral.* **1907**, *30*, 43.
(22) Keith, H. D.; Padden, F. J. *J. Polym. Sci.* **1959**, *39*, 123.
(23) Maillard, D.; Prud'homme, R. E. *Macromolecules* **2006**, *39*, 4272.
(24) Saracovan, I.; Keith, H. D.; Manley, R. St J.; Brown, G. R. *Macromolecules* **1999**, *32*, 8918.
(25) Ye, H.-M.; Xu, J.; Guo, B.-H.; Iwata, T. *Macromolecules* **2009**, *42*, 694.
(26) Shtukenberg, A. G.; Gunn, E.; Gazzano, M.; Freudenthal, J.; Camp, E.; Sours, R.; Rosseeva, E.; Kahr, B. *ChemPhysChem* **2011**, *12*, 1558.
(27) Owen, A. J. *Polymer* **1997**, *38*, 3705.
(28) Shahin, M. M.; Olley, R. H. *J. Polym. Sci., Part B: Polym. Phys.* **2002**, *40*, 124.
(29) Xu, J.; Guo, B.-H.; Zhang, Z.-M.; Zhou, J.-J.; Jiang, Y.; Yan, S.; Li, L.; Wu, Q.; Chen, G.-Q.; Schultz, J. M. *Macromolecules* **2004**, *37*, 4118.
(30) Xu, J.; Guo, B.-H.; Zhou, J.-J.; Li, L.; Wu, J.; Kowalczuk, M. *Polymer* **2005**, *46*, 9176.
(31) Shtukenberg, A.; Punin, Yu. *Optically Anomalous Crystals*; Kahr, B., Ed.; Springer: Dordrecht, 2007.
(32) Frondel, C. *Am. Mineral.* **1978**, *63*, 17.
(33) Gupta, A. S.; Arteaga, O.; Haislmaier, R.; Kahr, B.; Gopalan, V. *Chirality* **2013**, DOI: 10.1002/chir.22262.
(34) Addadi, L.; Berkovitch-Yellin, Z.; Weissbuch, I.; Lahav, M.; Leiserowitz, L.; Weinstein, S. *J. Am. Chem. Soc.* **1982**, *104*, 2075.
(35) Gunn, E.; Sours, R.; Benedict, J. B.; Kaminsky, W.; Kahr, B. *J. Am. Chem. Soc.* **2006**, *128*, 14234.
(36) Winchell, A. N. *The Optical Properties of Organic Compounds*; McCrone Research Institute: Chicago, 1987.
(37) Maillard, D.; Prud'homme, R. E. *Macromolecules* **2008**, *41*, 1705.
(38) Heaney, P. J. *Contrib. Mineral. Petrol.* **1993**, *115*, 66.
(39) Yu, L. *J. Am. Chem. Soc.* **2003**, *125*, 6380.

(40) Mareau, V. H.; Prud'homme, R. E. *Macromolecules* **2005**, *38*, 398.
(41) Nozue, Y.; Hirano, S.; Kurita, R.; Kawasaki, N.; Ueno, S.; Iida, A.; Nishi, T.; Amemiya, Y. *Polymer* **2004**, *45*, 8299.
(42) Kahr, B.; Shtukenberg, A. G.; Gunn, E.; Carter, D. J.; Rohl, A. L. *Cryst. Growth Des.* **2011**, *11*, 2070.
(43) Shtukenberg, A.; Freundenthal, J.; Gunn, E.; Yu, L.; Kahr, B. *Cryst. Growth Des.* **2011**, *11*, 4458.
(44) Kaminsky, W.; Glazer, A. M. *Z. Kristallogr.* **1997**, *212*, 283.
(45) Claborn, K.; Kahr, B.; Kaminsky, W. *CrystEngComm* **2002**, 252.
(46) Abe, H.; Doi, Y. *Macromolecules* **1996**, *29*, 8683.
(47) Reusch, E. *Ann. Phys. Chem.* **1869**, *138*, 628.
(48) Joly, G.; Billard, J. *J. Opt.* **1981**, *12*, 323.
(49) Arteaga, O.; Canillas, A. *Opt. Lett.* **2010**, *35*, 559.
(50) Arteaga, O., Mueller matrix polarimetry of anisotropic chiral media. Ph.D. Dissertation, Universitat de Barcelona, Spain, 2010.
(51) Yoon, D. K.; Yi, Y.; Shen, Y. Q.; Korblova, E. D.; Walba, D. M.; Smalyukh, I. I.; Clark, N. A. *Adv. Mater.* **2011**, *23*, 1962.
(52) Chen, D.; Maclennan, J. E.; Shao, R.; Yoon, D. K.; Wang, H. T.; Korblova, E.; Walba, D. M.; Glaser, M. A.; Clark, N. A. *J. Am. Chem. Soc.* **2011**, *133*, 12656.
(53) Hough, L. E.; Jung, H. T.; Kruerke, D.; Heberling, M. S.; Nakata, M.; Jones, C. D.; Chen, D.; Link, D. R.; Zasadzinski, J.; Heppke, G.; Rabe, J. P.; Stocker, W.; Korblova, E.; Walba, D. M.; Glaser, M. A.; Clark, N. A. *Science* **2009**, *325*, 456.